

Satellite-based detection and monitoring of phytoplankton blooms along the Oregon coast

S. M. McKibben,¹ P. G. Strutton,² D. G. Foley,³ T. D. Peterson,⁴ and A. E. White¹

Received 5 April 2012; revised 9 October 2012; accepted 10 October 2012; published 7 December 2012.

[1] We have applied a normalized difference algorithm to 8 day composite chlorophyll-*a* (CHL) and fluorescence line height (FLH) imagery obtained from the Moderate Resolution Imaging Spectroradiometer aboard the Aqua spacecraft in order to detect and monitor phytoplankton blooms in the Oregon coastal region. The resulting bloom products, termed CHL_{rel} and FLH_{rel}, respectively, describe the onset and advection of algal blooms as a function of the percent relative change observed in standard 8 day CHL or FLH imagery over time. Bloom product performance was optimized to consider local time scales of biological variability (days) and cloud cover. Comparison of CHL_{rel} and FLH_{rel} retrievals to in situ mooring data collected off the central Oregon coast from summer 2009 through winter 2010 shows that the products are a robust means to detect bloom events during the summer upwelling season. Evaluation of winter performance was inconclusive due to persistent cloud cover and limited in situ chl-*a* records. Pairing the products with coincident in situ physical proxies provides a tool to elucidate the conditions that induce bloom onset and identify the physical mechanisms that affect bloom advection, persistence, and decay. These products offer an excellent foundation for remote bloom detection and monitoring in this region, and the methods developed herein are applicable to any region with sufficient CHL and FLH coverage.

Citation: McKibben, S. M., P. G. Strutton, D. G. Foley, T. D. Peterson, and A. E. White (2012), Satellite-based detection and monitoring of phytoplankton blooms along the Oregon coast, *J. Geophys. Res.*, 117, C12002, doi:10.1029/2012JC008114.

1. Background

[2] Off the western margin of the continental United States, the Oregon coast represents the northern portion of the California Current system, a classic eastern boundary upwelling regime [Huyer, 1983]. Bloom dynamics have far-reaching effects from fueling a rich and diverse food web and associated fisheries harvests [Ware and Thomson, 1991, 2005] to driving rapid fluctuations in the air-sea flux of carbon dioxide [Evans *et al.*, 2011]. Blooms also affect the severity and spatial extent of hypoxic zones induced by bloom decomposition in preconditioned low-oxygen waters near the seafloor [Grantham *et al.*, 2004]. Harmful algal blooms are a regular

seasonal phenomenon in this region as well [Trainer *et al.*, 2010; Tweddle *et al.*, 2010] and can cause mass mortality of marine animals [Phillips *et al.*, 2011] or threaten human health through the consumption of shellfish contaminated with algal toxins [Trainer *et al.*, 2010]. The critical role that phytoplankton blooms play in each of these processes underscores the need to develop regionally based methods to identify and monitor blooms in Oregon's coastal waters.

[3] Blooms are classically defined as a "rapid increase of algal biomass over time among one, or a small number of, phytoplankton species" [Smayda, 1997]. Quantification of bloom events requires both a definition of what constitutes a bloom and time series measures of phytoplankton concentration. Bloom metrics are subjective, varying among research efforts according to the regional dynamics, sampling frequency, and methods applied. Threshold criteria, for instance, define blooms as any value that deviates from a median or other static value in a time series [Henson and Thomas, 2007b; Siegel *et al.*, 2002a; Wilson, 2003]. This approach is useful for the determination of bloom frequency and persistence in certain regimes, however it does not take into account regional or seasonal scales of variability. In Oregon's coastal waters, high-frequency shifts in wind stress induce rapid, short-lived (days) phytoplankton blooms [Hickey and Banas, 2003] and the magnitude of annual maximal in-water chl-*a* varies by a factor of two or greater (S. M. McKibben *et al.*, unpublished data, 2011). This variability at short and long time scales complicates efforts to define a static threshold

¹College of Earth, Ocean and Atmospheric Sciences, Oregon State University, Corvallis, Oregon, USA.

²Institute for Marine and Antarctic Studies, University of Tasmania, Hobart, Tasmania, Australia.

³Environmental Research Division, NOAA Southwest Fisheries Science Center, Pacific Grove, California, USA.

⁴Institute of Environmental Health, Division of Environmental and Biomolecular Systems, Oregon Health and Science University, Beaverton, Oregon, USA.

Corresponding author: S. M. McKibben, College of Earth, Ocean and Atmospheric Sciences, Oregon State University, 103 CEOAS Administration Bldg., Corvallis, OR 97330, USA.
(morgaine@coas.oregonstate.edu)

©2012. American Geophysical Union. All Rights Reserved.
0148-0227/12/2012JC008114

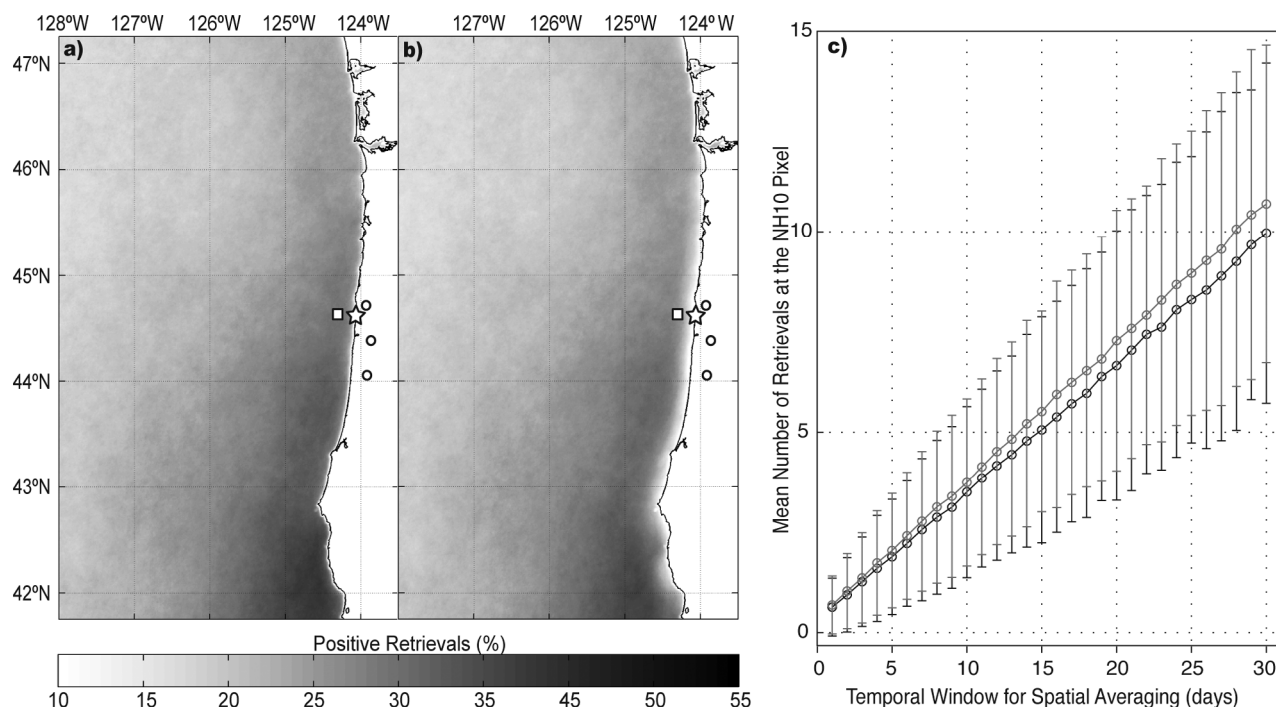


Figure 1. Percent positive retrievals off the Oregon and southern Washington coastlines for standard daily (a) CHL and (b) FLH from 2005 to 2010. Square indicates the location of the NH-10 mooring; star represents Newport, Oregon; circles show locations of streamflow gauging stations. (c) The mean number of retrievals obtained for daily CHL (black) and FLH (gray) at the pixel coincident with NH-10 as a function of the number of days elapsed for averaging. For both products, an 8 day time frame for composite averaging provides approximately 1–4 positive retrievals at NH-10.

for blooms. Iterative differences observed in phytoplankton concentration over short time frames (weeks or less) offer a more accurate bloom metric unaffected by longer-term signals. However, a continuous source of data at daily to weekly time scales, such as satellite data, is required.

[4] Satellite ocean color data provide synoptic, long-term time series coverage ideal for identification of bloom events. Two coincident ocean color products based on the optical properties chlorophyll-*a* (chl-*a*) are currently available from the Moderate resolution Imaging Spectroradiometer (MODIS) aboard the Aqua spacecraft: chl-*a* concentration (CHL), and fluorescence line height (FLH). Differences in chl-*a* observed by CHL or FLH over time provide a tracer of phytoplankton blooms and physical transport of phytoplankton biomass. We have developed and evaluated bloom products derived from normalized differences in ocean color imagery that are calculated on an iterative (daily) basis. The products were developed for Oregon's dynamic coastal waters, and their performance evaluated against in situ data, using methods that are applicable in any region with sufficient CHL and FLH coverage.

1.1. Regional Performance of CHL and FLH

[5] Bloom product development first requires region-specific consideration of standard product performance in terms of both accuracy and frequency of coverage. CHL

and FLH are proxies of chl-*a* absorption and emission, respectively. The empirical algorithm used to derive CHL is a polynomial best fit between satellite-observed radiance ratios and in situ chl-*a* measurements from predominantly clear open ocean waters [Werdell and Bailey, 2005]. Optically complex waters such as coastal regions are not well represented by these data, introducing error into CHL retrievals in these regimes [Claustre, 2003; Werdell et al., 2007]. In addition, both chl-*a* and colored dissolved organic matter (CDOM) absorb light strongly in the blue region of the visible spectrum which can lead to overestimates of CHL when CDOM is elevated [Claustre, 2003; Siegel et al., 2005]. River discharge is a distinctive feature of the Oregon coast [Chase et al., 2007; Wetz et al., 2006] and a prominent regional-scale control on satellite-derived distributions of CDOM [Siegel et al., 2002b]. Inflation of the CHL signal due to CDOM loading is likely in this region, particularly during times, or at sites, of high river outflow.

[6] FLH is derived from a line-height algorithm based on the spectral shape of water-leaving radiance in the red, as determined by solar-stimulated fluorescence emission of chl-*a* [Letelier and Abbott, 1996]. Unlike CHL, the FLH algorithm lacks bias from an in situ data set [Letelier and Abbott, 1996] and is not affected by CDOM loading [Hoge et al., 2003]. Chl-*a* fluorescence has long been used as a proxy of phytoplankton biomass in biological oceanography

[Kiefer and Reynolds, 1992], and FLH is also commonly applied as such, particularly in coastal regions with high CDOM loading [Behrenfeld *et al.*, 2009; Letelier and Abbott, 1996]. However, FLH is actually a function of both biomass and phytoplankton physiology that varies according to phytoplankton community composition, light and nutrient availability [Letelier and Abbott, 1996]. Therefore, FLH may vary as a function of physiological status in addition to changes in biomass [Behrenfeld *et al.*, 2009; Kiefer and Reynolds, 1992]. While FLH is less commonly applied to research than CHL, it has shown excellent promise in coastal bloom monitoring, particularly in the presence of CDOM [e.g., Hu *et al.*, 2004, 2005].

[7] The strengths and weaknesses of CHL and FLH can be considered complementary [International Ocean-Colour Coordinating Group, 2000], supporting usage and interpretation of these products in tandem. Enhancement of both CHL and FLH signals over the same area and time are most likely due to increased chl-*a*, while confounding signals, such as the influence of CDOM on CHL or physiology on FLH, may lead to differences between coincident CHL and FLH. Usage of either product alone may lead to falsely detected or overlooked blooms, so we have developed coincident bloom products based on both CHL and FLH.

1.2. Coupled Biological-Physical Dynamics of Oregon's Coastal Waters

[8] Criteria for regional bloom detection must take into account the dominant scales of physical forcing and subsequent biological response. Wind stress is a strong driver of physical and biological variability in Oregon's coastal waters and exhibits two seasonal modes. Roughly May through October (referred to hereafter as summer), phytoplankton blooms are induced by strong upwelling-favorable winds that drive Ekman transport of water offshore and bring cold, nutrient-rich water to the sunlit surface. Atmospheric oscillations drive alternations between upwelling, relaxation, or weakly downwelling favorable winds at short-term (2–6 days) and intraseasonal (15–40 days) intervals [Bane *et al.*, 2007]. Temperature and chl-*a* concentrations are tightly coupled with the intraseasonal variation in wind stress, responding on the order of a few days to 2 weeks, respectively [Bane *et al.*, 2007]. From roughly November through April (referred to hereafter as winter) strong downwelling-favorable winds are interspersed with short periods of relaxation or weak reversals. Deep, prolonged wind-driven mixing is assumed to keep chl-*a* relatively low throughout winter months.

[9] River discharge variability has similar seasonality and also affects bloom dynamics. Influxes of buoyant, particle-rich riverine water can stimulate or suppress blooms by affecting nutrient loading, light availability and water column stratification. In the summer, winds affect the position of the Columbia River Plume (CRP) relative to the Oregon coast: moving it southward and offshore during sustained upwelling events greater than roughly 2–3 days and closer to shore during sustained downwelling events, often with a second plume to the north [Hickey *et al.*, 2005]. In winter the CRP is shifted northward toward Washington [Hickey *et al.*, 2005] and Oregon's coastal rivers deliver large influxes of freshwater to the ocean from winter storms and spring snowmelt [Chase *et al.*, 2007; Wetz *et al.*, 2006].

Due to their influence on this region's bloom dynamics, metrics of wind stress and river discharge were included in the suite of in situ data used to evaluate bloom product performance and regional bloom phenology.

2. Data and Methods

2.1. Study Area

[10] Bloom product imagery was generated for the coastal and offshore waters of Oregon and southern Washington (41.5°N to 47.5°N and 123°W to 128°W; Figure 1a). Products were evaluated using in situ biological and physical proxies obtained from a mooring located at “NH-10,” a hydrographic station 10 miles offshore of Newport, Oregon (44.6°N and 124.3°W; square symbol in Figure 1a).

2.2. Data

2.2.1. In Situ Data

[11] All available fluorescence data collected at the NH-10 mooring were obtained as a metric of in-water bloom events. Raw fluorescence counts were measured once per second for 5 s each hour by a Wet Labs Combination Fluorometer and Turbidity Sensor (ECO-FLNTUSB) mounted one meter below the surface. These data were binned to daily averages but were not converted to calibrated units as the focus in this effort is to look at relative trends. Outliers greater than two standard deviations from the mean were removed. Records span August through November 2007, April through June 2008, and April through August 2009. The intervals are somewhat aperiodic due to variability in instrument performance (biofouling) and weather, which limited servicing and deployment opportunities.

[12] In situ measures of temperature, salinity, wind stress, and river discharge were also obtained for May 2009 through June 2010. This time frame represented the most continuous temperature and salinity records spanning summer to winter conditions at the NH-10 mooring. Temperature and salinity were recorded every 10 min at 2 m below the surface using a Sea-Bird Electronics 16 *plus* CTD and binned to daily averages. Raw wind data from the National Data Buoy Center's NWPO3 station at Newport, Oregon (star in Figure 1a) were used to derive daily wind stress using the method of Large and Pond [1981]. Streamflow records were acquired from the United States Geological Survey for 2005–2010 (<http://waterdata.usgs.gov/nwis/sw>) for three central coast rivers at the furthest downstream gauging station available (circles in Figure 1a). All three rivers have headwaters in the Coast Range, Oregon's westernmost mountain range, and drain into the Pacific. The daily median discharge of these rivers was calculated as a local measure of freshwater input.

2.2.2. Satellite Data

[13] MODIS data were obtained from the Ocean Biology Processing Group (OBPG; <http://oceancolor.nasa.gov>) as Level 2 (L2) hierarchical data format (HDF) files (processing version R2009.1, created by l2gen version 6.2.5) for the northeastern Pacific Ocean region (134°W to 121°W and 52°N to 34°N) from 2005 to 2010. L2 CHL and FLH swath data were extracted from the HDF files and masked according to the following OBPG-defined quality control flags: 1, atmospheric correction failure; 2, pixel is over land; 5, observed radiance very high or saturated; 10, cloud or ice

contamination; and 26, navigation failure (<http://oceancolor.gsfc.nasa.gov/VALIDATION/flags.html>). The data products were then mapped to an equal area 1 km (km) standard grid and temporally binned into daily files using arithmetic composite averaging, yielding two data sets of daily L3 CHL and FLH at 1 km resolution spanning 2005–2010.

[14] Two satellite images describing physical conditions were obtained to aid bloom product interpretation in section 3. MODIS L3 8 day 4 km resolution sea surface temperature imagery was obtained for 15–22 February 2006 from the OBPB. Archiving, Validation and Interpretation of Satellite Oceanographic (AVISO) sea surface height imagery at 0.25° (~28 km) resolution was obtained for 26 September 2009 (<http://las.pfeg.noaa.gov/oceanWatch/oceanwatch.php>).

2.3. Assessment of Regional CHL and FLH Accuracy and Coverage

[15] The standard CHL and FLH products and the bloom products based on them are considered proxies for the concentration of chl-a and relative change of chl-a, respectively. To evaluate this assumption and potential sources of error, we performed linear regression analysis of daily CHL and FLH retrievals and daily average in situ fluorescence at NH-10 to yield a first-order approximation of satellite data accuracy for the region. Daily mean CHL and FLH values were approximated by averaging values at the pixel coincident with NH-10, plus one pixel in each direction for statistical purposes (3x3 pixel area, or 9 km²). Outliers greater than two standard deviations from the time series mean were removed. The resulting CHL and FLH time series were then regressed against mean fluorescence at NH-10 on the corresponding day.

[16] Regional coverage of daily CHL and FLH is primarily determined by cloud cover, which, in turn, determines bloom product coverage. To evaluate the spatial extent of CHL and FLH coverage, maps describing the annual fraction of positive retrievals for each product were created. Values of one and zero were assigned to positive (valid = 1) and negative (invalid = 0) retrievals, respectively, in daily CHL and FLH imagery then temporally averaged over 2005–2010 to create percent coverage maps for each product.

2.4. Bloom Product Development

2.4.1. Algorithm

[17] Daily standard products were composite averaged, or temporally binned, over 8 day periods (the determination of this time frame is discussed in section 2.4.2) to attain a greater number of valid retrievals across the spatial domain of interest. The normalized difference between 8 day composite pairs comprises the bloom product algorithm:

$$\bar{X}_{rel} = \frac{\bar{X}_{current} - \bar{X}_{reference}}{\bar{X}_{reference}} \times 100\% \quad (1)$$

[18] Where \bar{X}_{rel} is the normalized relative difference between the pixel values at the same location in the two 8 day composites, $\bar{X}_{current}$ (e.g., $\bar{X}_{day9-16}$) and $\bar{X}_{reference}$ (e.g., \bar{X}_{day1-8}), and is repeated for each pixel in the defined coordinate plane. $\bar{X}_{current}$ and $\bar{X}_{reference}$ represent the 8 day composite pixel values for CHL ($\bar{C}_{current}$, $\bar{C}_{reference}$) and FLH

($\bar{F}_{current}$, $\bar{F}_{reference}$), respectively. CHL and FLH exhibit lognormal and normal distributions over time and space, respectively. As a result, the geometric mean was applied to calculate $\bar{C}_{current}$ and $\bar{C}_{reference}$ and the arithmetic mean was used to calculate $\bar{F}_{current}$ and $\bar{F}_{reference}$. Equation (1) is applied at daily intervals yielding a daily bloom product derived from up to 16 prior days of satellite observations.

2.4.2. Regional Assessment of Biological Variability and Satellite Coverage

[19] Two factors were evaluated to determine the 8 day composite time frame for equation (1): observed temporal scales of in situ biological variability and the frequency of satellite coverage at NH-10. First, biological variability was assessed through autocorrelation analysis of the three in situ NH-10 fluorescence time series for 2007, 2008, and 2009. Temporal decorrelation scales for each time series, a measure of bloom persistence during the time frame of observation, were defined as the lag value closest to the 95% significance level [Glover *et al.*, 2011].

[20] Second, the percent of positive retrievals achieved by standard daily CHL and FLH from 2005 to 2010 was assessed by determination of the average gap observed between positive retrievals at NH-10 for CHL. Average gap length was determined by extracting the pixel value coincident with NH-10 from the daily CHL coverage maps described in section 2.3, then summing the total number of consecutive negative retrievals between each positive retrieval. The average gap length and its standard deviation, median, and mode were then calculated.

2.5. Evaluation of Bloom Product Performance in Coastal Waters

[21] The temporal coverage provided by the 8 day time frame in coastal regions was evaluated for CHL_{rel} by binning satellite data into five regions of equal area: A through E, 1° of latitude by 0.5° longitude west of the coast. North-south bin size was based on observed patterns in latitudinal CHL variability induced by north-south gradients in wind stress, solar insolation, and bathymetry [Henson and Thomas, 2007a; Tweddle *et al.*, 2010; Venegas *et al.*, 2008]. East-west bin size spans the continental shelf where CHL is greatest [Henson and Thomas, 2007b; Venegas *et al.*, 2008] and percent retrievals for daily MODIS CHL and FLH are highest (Figures 1a and 1b). The annual median percentage and standard deviation of positive retrievals for each coastal region was calculated and plotted in time.

[22] As a metric of daily bloom events observed in the vicinity of NH-10 via satellite, daily CHL_{rel} and FLH_{rel} time series were created using the methods described in section 2.3 for daily CHL and FLH at NH-10. Time series analysis of CHL_{rel} and FLH_{rel} relative to in situ parameters was then applied to assess product accuracy and determine physical drivers of observed blooms. All time series were first separated into upwelling and downwelling, or summer and winter, seasons. Broad definitions of these seasons were mentioned previously; on an annual basis they can be identified by spring and fall transition dates based on the onset and termination, respectively, of cumulative upwelling (CU) conditions [Pierce *et al.*, 2006]. The CU index integrates annual wind stress beginning on 1 January and defines the spring and fall transitions as the start date of net upwelling

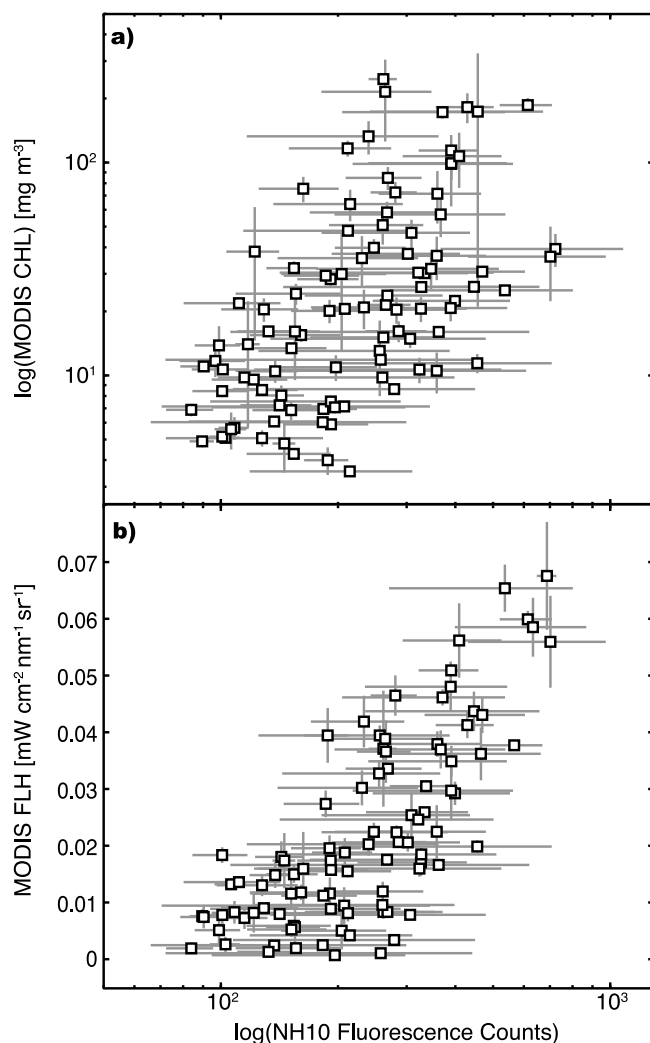


Figure 2. Linear regression of daily mean raw fluorescence at the NH-10 mooring and daily mean (a) chlorophyll-a concentration (CHL; $r^2 = 0.34$) and (b) fluorescence line height (FLH; $r^2 = 0.56$) products averaged over a 9 km² region centered at the NH-10 mooring. The error bars in the x and y directions indicate 1 standard deviation from the mean raw fluorescence and satellite values, respectively.

and downwelling conditions, respectively. In 2009–2010, summer spanned 14 May to 11 October 2009 and winter spanned 13 October 2009 through 13 June 2010. Next, the time series were cross correlated with temperature, salinity, wind stress, and river discharge to quantify the degree to which observed bloom events are related to in situ parameters. Results were considered significant if above the 95% significance level [Glover *et al.*, 2011] and if lag values were less than 16 days, the time frame spanned by the bloom products.

[23] Compared to in situ time series, daily values of CHL_{rel} and FLH_{rel} at NH-10 are based on calculations that span up to 16 days and data points are aperiodic, particularly in winter. A secondary measure of bloom product performance was evaluated as these factors may negatively affect cross-correlation analysis, which works best on continuous time series at equivalent time scales [Glover *et al.*, 2011]. The

product algorithm (equation (1)) was applied to daily in situ fluorescence records from 2007 and 2009 to yield a proxy of “expected” bloom activity at NH-10 then compared to blooms observed via satellite. Data from 2008 were not included as the in situ record was comparatively short and satellite coverage was poor during that time. Metrics of expected and observed blooms were evaluated over time, as well as relative to each other.

3. Results and Discussion

3.1. Regional CHL and FLH Coverage and Accuracy

[24] The spatial coverage of daily CHL and FLH (Figures 1a and 1b) exhibits a latitudinal gradient with the highest percent retrievals ($\sim 35\%$) in the south. Onshore to offshore, coverage decreases to approximately 15–20% beyond the shelf break. Relative to CHL, daily FLH coverage is roughly 3–5% lower, and nearshore coverage within about 15 km of shore is reduced (Figure 1b). Coverage at the pixel coincident with NH-10 averages 29% and 27% for CHL and FLH, respectively.

[25] Relative to CHL, FLH explained a greater percent of the in situ variance (34%, 56%, respectively, at the 95% significance level; Figure 2), supporting the interpretation of FLH as an indicator of phytoplankton biomass despite the known impact of variable physiology on this product [Behrenfeld *et al.*, 2009]. The weaker relationship observed between CHL and in situ fluorescence at NH-10 may be a consequence of reduced CHL algorithm performance in coastal regions [Werdell *et al.*, 2007]. The significance of the fit between the standard products and in situ fluorescence is also impacted by errors in satellite-based estimates of chl-a which include atmospheric correction methods applied during L2 processing, sensor accuracy and calibration, solar zenith angle at time of satellite flyover, physiological variability of phytoplankton assemblages, and the selected application of quality control flags during L3 processing. In addition, CHL, FLH, and in situ fluorescence are different optical proxies based on the absorbance, and passive and stimulated fluorescence of chl-a, respectively. While we have only evaluated the goodness of fit for data records immediately around the NH-10 mooring, our results (Figures 1 and 2) indicate that daily MODIS CHL and FLH products are a sound foundation for phytoplankton bloom detection in this region.

[26] Linear regression of coincident satellite retrievals and in situ fluorescence provides both an approximation of product accuracy and a baseline for intercomparison of daily CHL and FLH retrievals (Figure 2). Mooring observations at NH-10 and coincident pixel retrievals are both measured in an Eulerian frame of reference, meaning that observed chl-a variability is due to growth, decay, and advection of surface blooms. As such, the in situ NH-10 records are a reasonable first-order approximation of expected chl-a concentrations and scales of variability that would be observed if daily satellite retrievals at the pixel coincident with NH-10 approached 100%.

3.2. Bloom Product Algorithm Development

[27] Scales of biological variability (Figure 3) and satellite data frequency (Figure 1c) were the primary guiding factors in determining the 8 day composite time frame applied to the

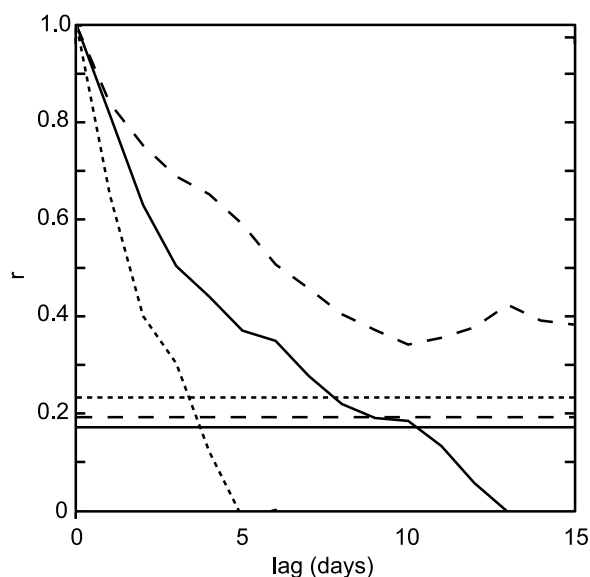


Figure 3. Temporal decorrelation scales of daily mean raw fluorescence at the NH-10 mooring for August through November 2007 (long-dashed line; $n = 110$), April through July 2008 (short-dashed line; $n = 77$), and April through August 2009 (solid line; $n = 139$). Horizontal lines are 95% confidence intervals for each year.

bloom product algorithm (equation (1)). Observed bloom decorrelation scales were 3–10 days at NH-10 in 2008 and 2009 (Figure 3). These values are similar to previous studies in the northern California Current System that report in situ decorrelation scales of 2.5 [Abbott and Letelier, 1999] and less than 4.5 days (S. Frolov et al., Monitoring of harmful algal blooms in the era of diminishing resources: A case study of the U.S. West Coast, submitted to *Harmful Algae*, 2012) based on drifter and mooring chl-a records, respectively. With the exception of data collected in April, the 2008 and 2009 time series both covered summer months when chl-a values and variability were highest. In contrast, 2007 decorrelation scales were greater than 15 days (Figure 3), which is expected given this time series predominately spanned the transition from late summer to winter when fluorescence values remain comparatively low and constant. These time series exhibit the broad range of temporal variability, from daily to weekly, seasonal, and interannual scales, characteristic of this dynamic region.

[28] Frequency of coverage, as measured by the average gap observed between positive (valid) CHL retrievals at the pixel coincident with NH-10, is 4.81 days with a standard deviation of 4.80 days. The distribution is skewed toward zero with a median of 3 days and a mode of 1 day; a 7 day and 11 day gap mark the 75th and 90th percentile of this distribution, respectively. Coupled with the 3–10 day bloom decorrelation scales, these results indicate that an 8 day span is an appropriate choice for temporal binning of the current ($\bar{X}_{current}$) and reference ($\bar{X}_{reference}$) composites. This time frame lies approximately in the middle of where these ranges overlap and is also a standard time window for OBPB ocean color products. Over an 8 day period, composites

permit an average of 1 to 4 retrievals over a 9 km² region centered at NH-10 (Figure 1c).

[29] Consistent with nearshore spatial trends in CHL and FLH coverage (Figures 1a and 1b), coastal CHL_{rel} and FLH_{rel} coverage is best in the south and successively decreases toward the north (Figures 4a–4e). Annual percent positive retrievals in all regions are highly variable throughout the 5 year data set (Figures 4a–4e), with the greatest coverage in summer. Together, Figures 1 and 4 show that optimal product coverage coincides with Oregon's greatest bloom activity: in coastal waters during summer upwelling season.

3.3. Bloom Product Imagery Interpretation

[30] Equation (1) produces daily bloom products (Figures 5c and 5f) from relative differences between successive 8 day current (Figures 5a and 5d) and reference (Figures 5b and 5e) composites. Where standard CHL and FLH describe the distribution of phytoplankton standing stocks in terms of bulk chl-a concentration, the corresponding CHL_{rel} and FLH_{rel} products describe the variability in bulk chl-a over time, targeting the initial growth or advective transport of nascent phytoplankton blooms. Daily coverage of CHL and FLH (Figure 1) influences the accuracy of the bloom products by determining the number of data points available for composite averaging of any given pixel ($\bar{X}_{current}$, $\bar{X}_{reference}$). While compositing can dampen observed variability at temporal scales less than 8 days, in situ fluorescence decorrelation scales (Figure 3) and mean retrievals at NH-10 (Figure 1c) indicate that 8 day running composites are sufficient to capture changes in phytoplankton biomass, yet still contain valuable information regarding shorter-term mesoscale variability on the order of weeks to months [Haury et al., 1978; O'Reilly et al., 1998].

[31] As expected, coincident CHL_{rel} and FLH_{rel} imagery exhibit both similarities and differences in the resultant spatial patterns and relative magnitude of bloom signals (i.e., regions of positive relative change shown by red coloration on Figures 5c and 5f). For instance, Figures 5c and 5f show bloom signals of similar magnitude and spatial extent coincident with decreased alongshore sea surface height anomalies, indicating the signals are likely the result of upwelling-induced blooms. In contrast, Figure 6a shows a large positive CHL_{rel} signal inshore of the shelf break near the Columbia River mouth and Juan de Fuca straight that is coincident with warmer sea surface temperature (SST) (Figure 6c), yet is not apparent in FLH_{rel} (Figure 6b). Elevated SST near points of significant freshwater discharge is suggestive of freshwater intrusions, and the shelf break is a retentive feature known to keep this region's exceptionally high river outflow [Wetz et al., 2006] confined to shallow shelf waters [Hickey and Banas, 2008]. The strong bloom signals in CHL_{rel} may be driven by winter storm-induced surges of freshwater rich in CDOM rather than active phytoplankton blooms. Differences in coincident bloom product imagery, such as these, are potentially due to confounding signals in CHL_{rel} or FLH_{rel} and merit future work.

3.4. Bloom Product Performance: A Case Study of the Central Oregon Coast

[32] In time series data at NH-10, bloom events are evident as well defined, or successive series of, peaks in CHL_{rel}

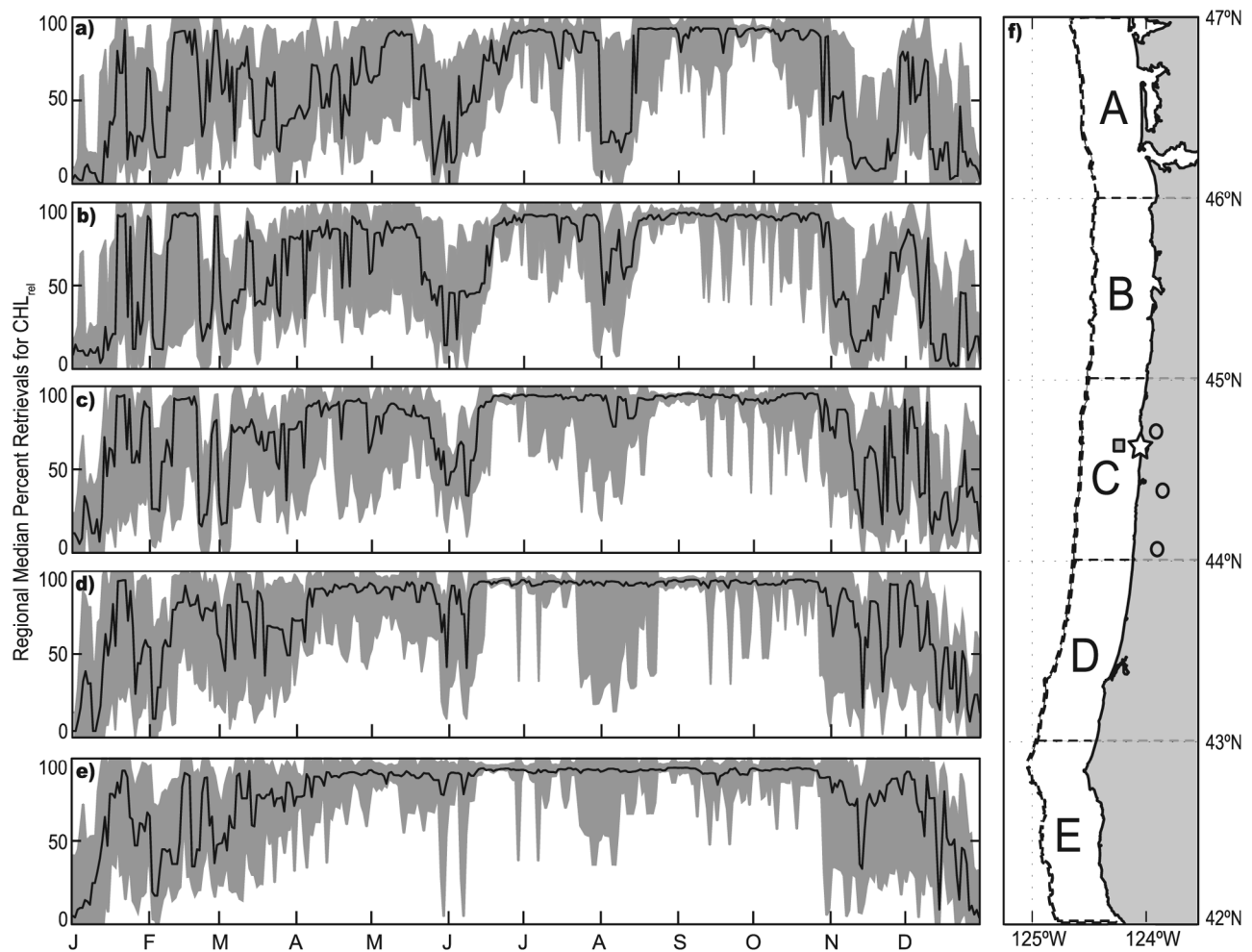


Figure 4. (a–e) The median temporal coverage (solid black lines) and standard deviation (gray shading) of CHL_{rel} from 2005 to 2010 in (f) correspondingly labeled regions A through E. Spatial bins for each region and locations of data collection are detailed in Figure 4f: square indicates the location of the NH-10 mooring; star represents Newport, Oregon; circles show locations of streamflow gauging stations.

and FLH_{rel} (Figure 7a). Summer bloom events are detected by both CHL_{rel} and FLH_{rel} at the same time scales relative to each other ($r = 0.57$; Table 1). Plots of coincident central coast time series (Figures 7a–7d) indicate significant correlation between wind stress, chl-a proxies, and all in situ physical parameters, with the exception of river discharge during summer (correlations summarized in Table 1). Winter time gaps in satellite coverage at NH-10 spanned several weeks (Figure 7a, January through April), precluding correlation analysis during this season.

[33] When compared to “expected” bloom activity at NH-10 (Figure 8), CHL_{rel} and FLH_{rel} in 2007 detected nearly all blooms predicted by the in situ data, describing 52% and 38% of the in situ bloom variance. Two peaks consisting of single points in mid and late October of 2007 (Figure 8a) are likely attributable to low sample retrievals. In 2009, 10% and 28% of the variance was captured. This lower variance is due to a bloom event observed in late May of 2009 by both satellite products, but not observed at the mooring (Figure 8b). Patchiness may explain this disparity between satellite and moored records: in a 9 km² region an observed bloom may occur in, or be advected into, a subset of

retrieved pixels, yet not reach the mooring. Overall, both bloom products successfully observed all blooms predicted by the in situ data, with the exception of an event in August of 2009 that was detected by FLH_{rel} only (Figure 8b).

3.5. Central Coast Bloom Phenology

[34] Observed seasonal and intraseasonal variability in central coast biological and physical parameters from May of 2009 through June 2010 (Figure 7) can be summarized as follows. In summer, coastal river flow is significantly reduced, standing stocks of chl-a are elevated, and predominantly upwelling-favorable winds are interspersed with reversal and relaxation events. Peaks in bloom products and in situ fluorescence reliably follow surface intrusions of cooler, more saline waters induced by upwelling. Winter exhibits high coastal river outflow and is dominated by strong downwelling winds that are separated by periods of relaxation and weak reversals. Biological-physical relationships in winter are inconclusive due to the absence of in situ fluorescence records at NH-10 and inconsistent data retrieval in the bloom products caused by frequent cloud cover.

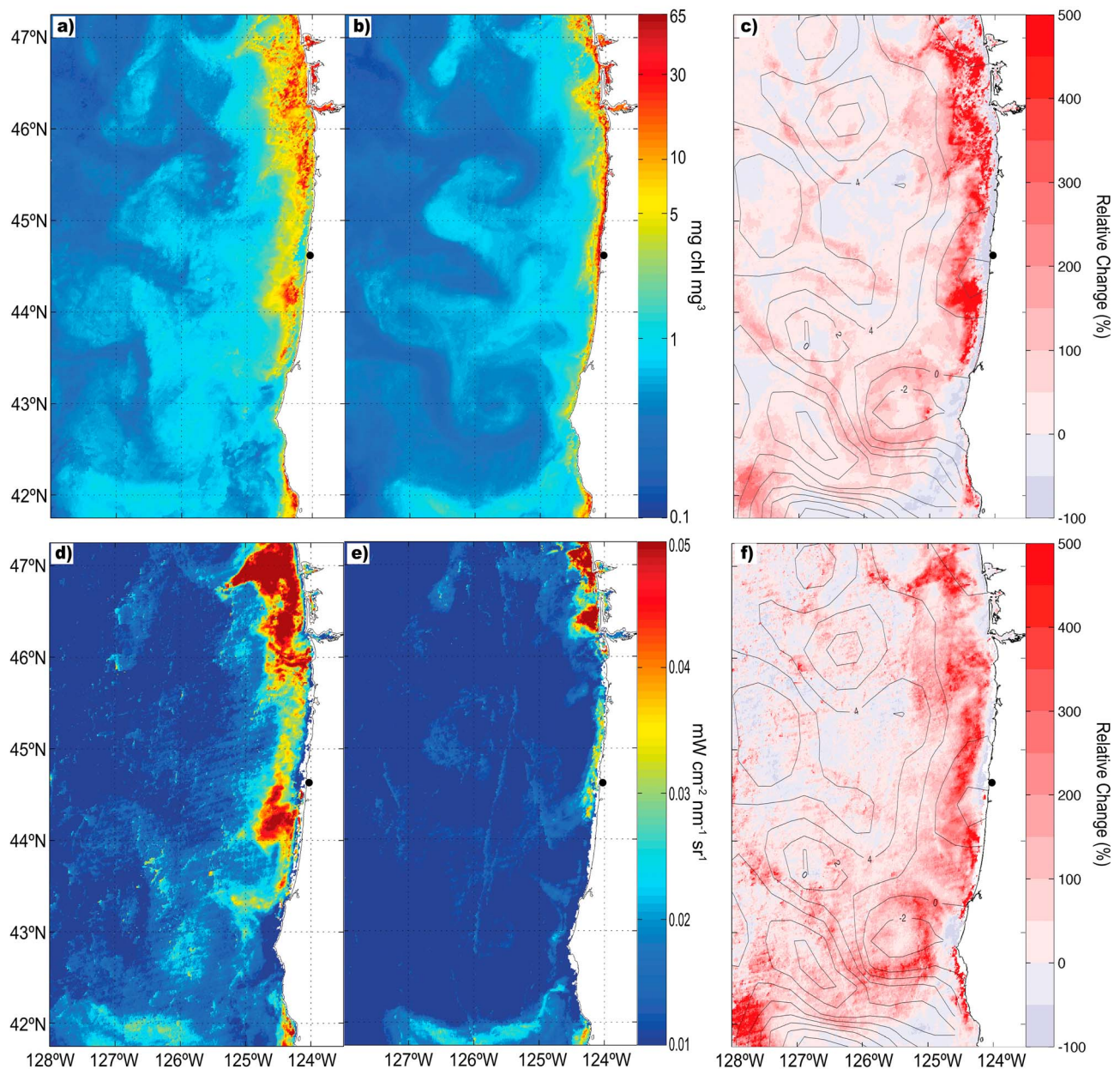
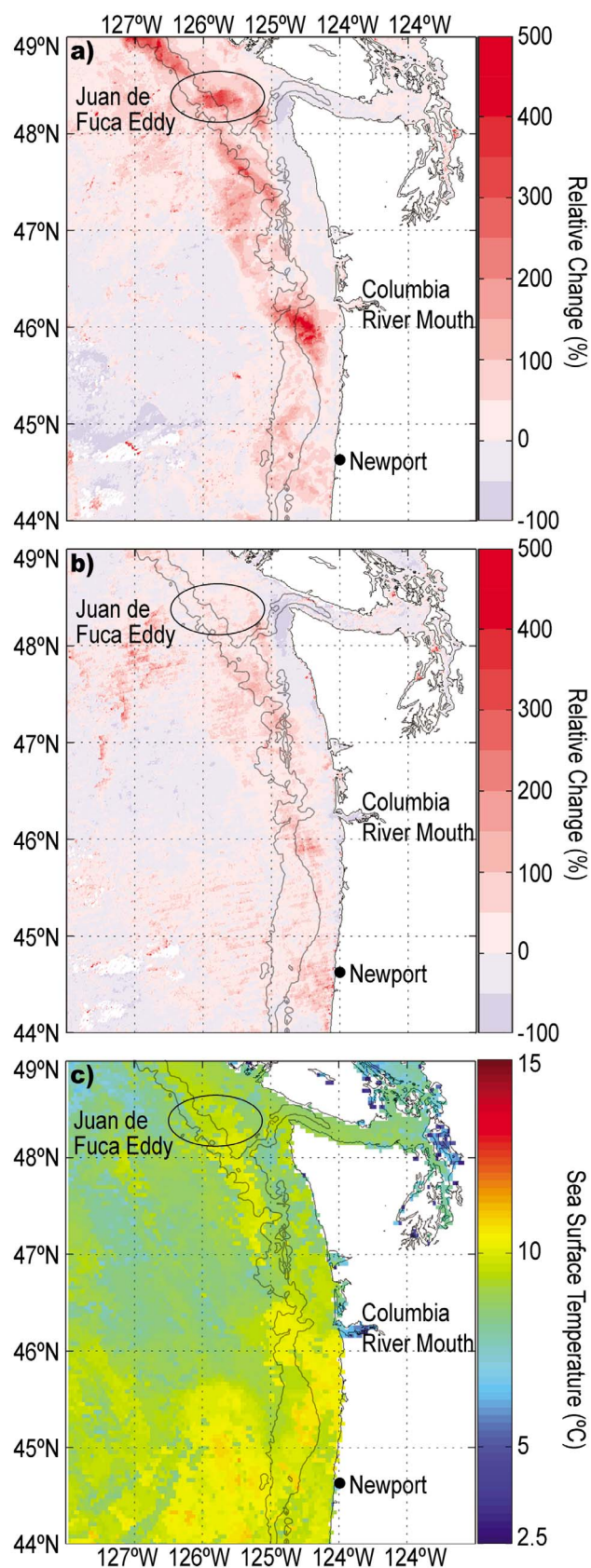


Figure 5. Sample of “current” ((a and d) 23–30 September 2009) and “reference” ((b and e) 15–22 September 2009) 8 day composite imagery for standard CHL (top row) and FLH (bottom row) products. Bloom products are created by subtracting the reference from the current composite, then normalizing to the reference. Resulting (c) CHL_{rel} and (f) FLH_{rel} imagery displays the pixel-by-pixel relative percent change observed in CHL and FLH over a 16 day time frame. Bloom products in Figures 5c and 5f are overlaid with 0.25° (~ 28 km) resolution AVISO sea surface height (SSH) anomaly contours at 2 cm intervals for the week of 26 September 2009. Anomaly coloration is employed with positive relative differences in shades of red and negative differences in shades of blue. White indicates pixels lacking data due to quality control flags. Notable features in Figures 5c and 5f include bloom signals coincident with alongshore depressed SSH, an indicator of coastal upwelling, and offshore mesoscale circulation features.

[35] In the summer, upwelling favorable wind stress rapidly induces coupled cooling and increased salinity at NH-10 in 1–2 days (Table 1). Increased in situ fluorescence lags upwelling wind and cooling surface waters by 5–6 days, respectively. Lag times between the bloom products and these physical variables are less consistent and longer, ranging from 6 to

9 days (Table 1). This was expected as daily bloom product values are based on a calculation that spans 16 days and cloud cover can cause sporadic data retrieval during that time. Overall, the bloom products performed best during summer months when standing stocks of chl-a were highest.



[36] Winds also exert strong, yet variable, control on in-water parameters in the winter. Prolonged deep winter mixing and declining air temperatures steadily decrease water temperature until roughly January when both stabilize (Figures 7b and 7c). Unlike summer, temperature and salinity are largely decoupled as downwelling winds push water shoreward, keeping salinity relatively constant in well-mixed surface waters (Tables 1 and 2). Drops in salinity follow relaxation and weak reversal events that allow the pooling of fresh, buoyant river outflow which arrives at NH-10 approximately a day after relaxation events (Figures 7c and 7b and Table 1). Downwelling favorable winds are strongly associated with high river discharge (Table 1), indicating that they coincide with winter rainstorms west of the Coast Range. Prevalent coastal river outflow in winter (Figure 7d) may fuel significant winter productivity [Wetz *et al.*, 2006] and affect CHL accuracy through CDOM loading [Siegel *et al.*, 2005]. However, due to poor satellite coverage and a lack of in situ chl-a records, only one winter bloom was confirmed using in situ data in 2007 (Figure 8a, November). Ongoing efforts to enhance autonomous data collection should allow further constraint of winter bloom dynamics in this region.

3.6. Product Applications

[37] CHL_{rel} and FLH_{rel} provide a powerful platform for remote identification and monitoring of phytoplankton blooms in response to physical and chemical forcing. These products target the critical initiation phase of potential blooms, allowing consideration of the mechanisms that trigger blooms. In combination with maps of absolute concentration, they can also be used to evaluate bloom persistence. Dissimilar CHL_{rel} and FLH_{rel} signals may prove useful to identify error in products, diagnose CDOM intrusions, or, when viewed in parallel with satellite altimetry, show enhancement or transport of phytoplankton biomass via mesoscale features (e.g., Figures 5c, 5f, and 6a).

[38] Improvement of bloom detection accuracy may be achieved by deriving additional bloom products from other satellite chl-a proxies. For instance, development of regionally tuned CHL algorithms [e.g., Werdell *et al.*, 2007] would yield region-specific bloom products. Alternatively, chl-a products based on semianalytical inversion algorithms [e.g., Hoge *et al.*, 1999; Maritorena *et al.*, 2002], which separate chl-a absorption from CDOM and detrital particle absorption, could yield bloom products that are theoretically free of confounding CDOM signals. Methods proposed by Behrenfeld *et al.* [2009] could be applied at a regional scale to develop a fluorescence-based bloom product that is corrected for

Figure 6. Bloom product output for 22 February 2006 (15–22 February relative to 7–14 February). Note the stronger signal in (a) CHL_{rel} relative to (b) FLH_{rel} near the mouth of the Columbia River and offshore of the Washington and Canadian coasts, particularly the Juan de Fuca Eddy which is offshore of the Juan de Fuca straight. Contours are 200 and 1000 m isobaths. (c) Four km 8 day MODIS sea surface temperature imagery was obtained for 15–22 February 2006 as a coincident metric of freshwater outflow. Warmer water temperatures (Figure 6c) are associated with the positive CHL_{rel} signal.

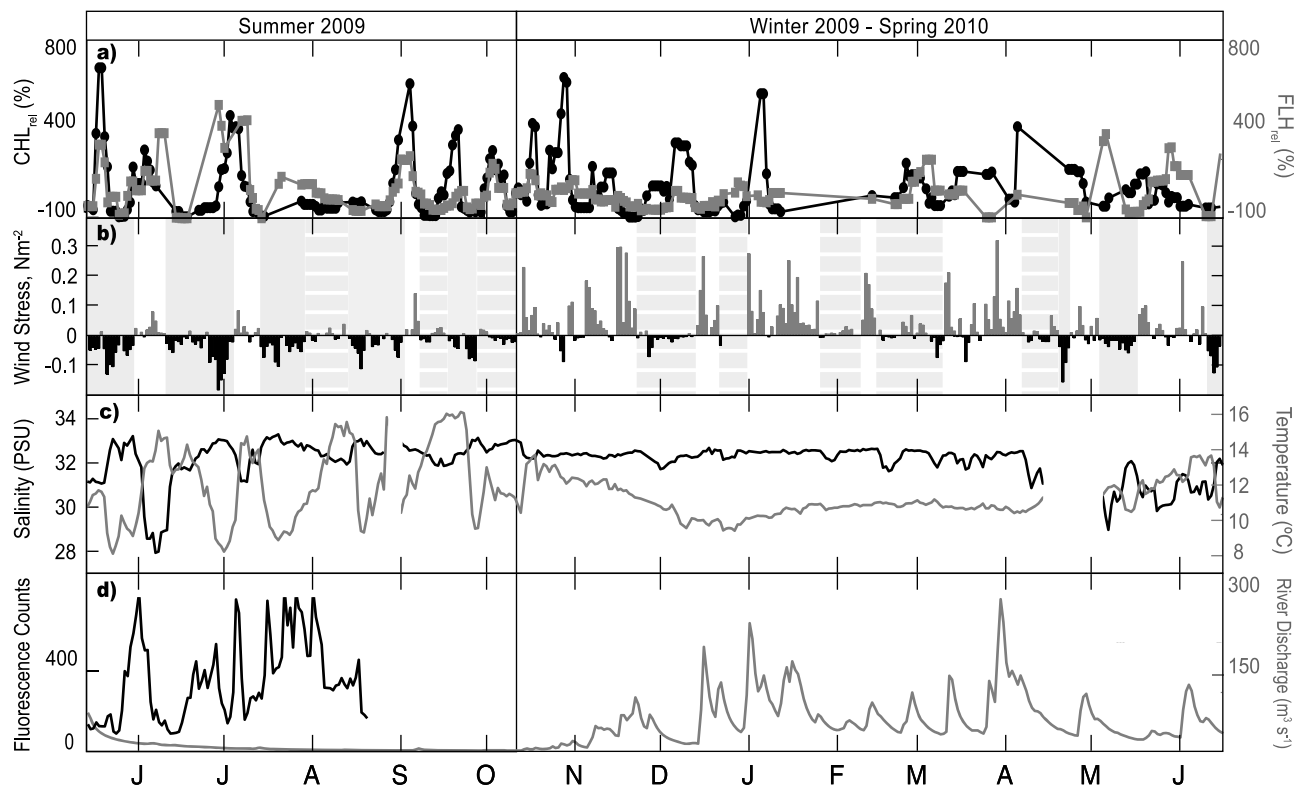


Figure 7. Daily biological and physical parameters for the central Oregon coast from May 2009 through June 2010. (a) Mean CHL_{rel} (black) and FLH_{rel} (gray) across a 3×3 pixel region centered on NH-10. Dots indicate positive satellite retrievals. (b) Daily wind stress vectors in the northward (gray bars) or southward (black bars) direction at Newport, Oregon. Upwelling, downwelling, and relaxation events were defined as 4 or more days of wind stress values that were predominantly negative (southward, solid gray), positive (northward, white), or between $\pm 0.05 \text{ N m}^{-2}$ (striped gray), respectively. (c) Salinity (black) and temperature (gray) at the NH-10 mooring. (d) NH-10 mooring fluorescence (black) and daily median river discharge (gray) from central coast gauging stations. Summer and winter divisions of time series based on spring and fall transition dates are indicated at the top.

Table 1. Cross-Correlation Coefficients (r) and Corresponding Time Lags Between the Central Oregon Coast Biological and Physical Time Series Shown in Figure 7^a

	Summer 2009					Winter 2009		
	Wind Stress	NH-10 Temperature	NH-10 Salinity	River Discharge	FLH_{rel}	Wind Stress	NH-10 Temperature	NH-10 Salinity
<i>Biophysical Cross-Correlation Results</i>								
CHL_{rel}^b	-0.24 (8)	-0.26 (6)	0.30 (8)	NS	0.57 (0)	NA	NA	NA
FLH_{rel}^b	-0.38 (9)	-0.34 (7)	0.31 (9)	NS	-	NA	NA	NA
NH-10 fluorescence	-0.39 (6)	-0.43 (5)	0.62 (5)	NS	-	NA	NA	NA
<i>Physical Cross Correlation Results</i>								
NH-10 temperature	0.57 (2)	-	-	-	-	NS	-	-
NH-10 salinity	-0.41 (1)	-0.46 (0)	-	-	-	0.28 (0)	NS	-
River discharge	-0.28 (-7)	NS	NS	-	-	0.49 (1)	NS	0.24 (2)

^aSummer (14 May to 11 October 2009) and winter (12 October 2009 to 13 June 2010) are upwelling and downwelling seasons, respectively, based on net wind stress. "NS" indicates insignificant correlations, and a hyphen indicates values reported elsewhere in the table or autocorrelation values reported in Table 2. NA indicates insufficient data were available for cross-correlation analysis. Strong cloud cover precluded correlation analysis with satellite data during winter, and fluorescence at the NH-10 mooring were not available for winter or the latter part of summer. Here r represents the correlation coefficient based on cross-correlation analysis; greatest correlation is indicated by ± 1 and least by 0. All correlations reported at the 95% significance level according to the n values reported in Table 2. Each x parameter (top row) follows the y (first column) according to the lag (in days) reported in parentheses. For example, fluorescence at NH-10 and wind stress are significantly negatively correlated ($r = -0.39$) at a lag of 6 days; that is, high fluorescence values observed at the mooring most frequently occur 6 days after strong southward (upwelling-favorable) wind stress.

^b CHL_{rel} and FLH_{rel} refer to time series of the CHL- and FLH-based satellite bloom product values, respectively, averaged over a 9 km^2 box centered on NH-10.

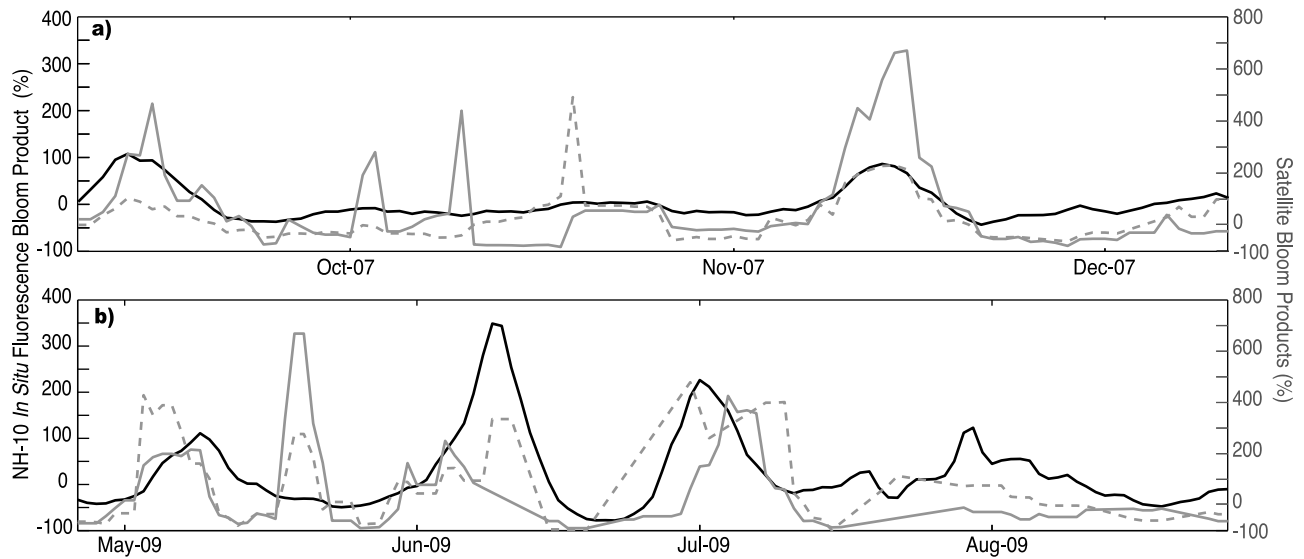


Figure 8. Bloom product algorithm (see equation (1)) applied to daily mean raw fluorescence (solid black) as a metric of expected bloom events at the NH-10 mooring for (a) 2007 and (b) 2009. Gray lines show blooms observed by coincident CHL_{rel} (solid gray) and FLH_{rel} (dashed gray) across a 3×3 pixel box centered on NH-10. Note difference in x and y scales.

factors such as irradiance and chl-a concentration that are known to introduce variability into the FLH signal. All of these efforts merit future study in this region and are applicable to similar regimes as well.

4. Conclusions

[39] The bloom products developed and analyzed herein have shown that the relative change in CHL and FLH over time effectively identifies nascent blooms in Oregon's coastal waters. Both products were shown to provide sufficient spatial coverage for Oregon's coastal regions and to accurately detect blooms in central coast waters, particularly during productive summer months. Product imagery identifies bloom events in space and daily changes in imagery describe bloom

evolution over time, providing a way to monitor the onset and subsequent advection of blooms. If based on a thorough local assessment of temporal and spatial satellite coverage and compared to in situ data as we have done here, these products will also be useful in other regions to address the phenology of phytoplankton growth and biological/physical coupling.

[40] **Acknowledgments.** This study was supported by National Oceanic and Atmospheric Administration (NOAA) grant NA07NOS4780195 from the Monitoring and Event Response for Harmful Algal Blooms (MERHAB) program and NA08NES4400013 to the Cooperative Institute for Oceanographic Satellite Studies. This is MERHAB publication 165. Thank you to Stephen Pierce and Wiley Evans for data provided and to Michelle Wood for helpful discussion. Initial concept of chlorophyll anomaly product development for Oregon was supported by NOAA Oceans and Human Health grant NA04OAR4600202. The statements, findings, conclusions, and recommendations are those of the authors and do not

Table 2. Decorrelation Scales for the Central Oregon Coast Biological and Physical Time Series Shown in Figure 7^a

	Summer 2009		Winter 2009–2010	
	Decorrelation Scale (Days)	n^b (Days)	Decorrelation Scale (Days)	n^b (Days)
CHL_{rel}^c	± 2	119	± 3	150
FLH_{rel}^c	± 2	114	± 6	147
NH-10 fluorescence	± 7	99	-	-
NH-10 temperature	± 7	148	NS	225
NH-10 salinity	± 7	146	NS	224
Wind stress	± 3	151	± 3	247
River discharge	NS	151	NS	248

^aSummer (14 May to 11 October 2009, 151 total days) and winter (12 October 2009 to 13 June 2010, 245 total days) are upwelling and downwelling seasons, respectively, based on net wind stress. All decorrelation scales are reported at the 95% significance level according to their corresponding n value listed in the table. "NS" indicates insignificant correlation. Fluorescence data from the NH-10 mooring were not available for winter or the latter part of summer (indicated by hyphens).

^bThe n values represent the number of data points that comprise each time series. All time series are daily scale; hourly mooring data were daily averaged. Here n is often less than the total number of days in the season due to cloud cover in satellite data or discontinuous in situ records. For instance, percent coverage of the bloom products at NH-10 was greater during summer at 75–79% (114–119 of 151 possible days) compared to 60–61% during winter (147–150 out of 245 possible days).

^c CHL_{rel} and FLH_{rel} refer to time series of the CHL- and FLH-based satellite bloom product values, respectively, averaged over a 9 km^2 box centered on NH-10.

necessarily reflect the views of the National Oceanic and Atmospheric Administration or the Department of Commerce.

References

- Abbott, M. R., and R. M. Letelier (1999), Algorithm theoretical basis document chlorophyll fluorescence (MODIS product number 20), NASA Goddard Space Flight Center, Greenbelt, Md. [Available at <http://modis.gsfc.nasa.gov/data/atbd/>].
- Bane, J. M., Y. H. Spitz, R. M. Letelier, and W. T. Peterson (2007), Jet stream intraseasonal oscillations drive dominant ecosystem variations in Oregon's summertime coastal upwelling system, *Proc. Natl. Acad. Sci. U. S. A.*, **104**(33), 13,262–13,267, doi:10.1073/pnas.0700926104.
- Behrenfeld, M. J., T. K. Westberry, E. S. Boss, R. T. O'Malley, D. A. Siegel, J. D. Wiggert, B. Franz, C. McClain, G. Feldman, and S. C. Doney (2009), Satellite-detected fluorescence reveals global physiology of ocean phytoplankton, *Biogeosciences*, **6**, 779–794, doi:10.5194/bg-6-779-2009.
- Chase, Z., P. G. Strutton, and B. Hales (2007), Iron links river runoff and shelf width to phytoplankton biomass along the U.S. West Coast, *Geophys. Res. Lett.*, **34**, L04607, doi:10.1029/2006GL028069.
- Claustre, H. (2003), The many shades of ocean blue, *Science*, **302**(5650), 1514–1515, doi:10.1126/science.1092704.
- Evans, W., B. Hales, and P. G. Strutton (2011), Seasonal cycle of surface ocean $p\text{CO}_2$ on the Oregon shelf, *J. Geophys. Res.*, **116**, C05012, doi:10.1029/2010JC006625.
- Glover, D., W. Jenkins, and S. Doney (2011), *Modeling Methods for Marine Science*, Cambridge Univ. Press, New York, doi:10.1017/CBO9780511975721.
- Grantham, B. A., F. Chan, K. J. Nielsen, D. S. Fox, J. A. Barth, A. Huyer, J. Lubchenco, and B. A. Menge (2004), Upwelling-driven nearshore hypoxia signals ecosystem and oceanographic changes in the northeast Pacific, *Nature*, **429**, 749–754, doi:10.1038/nature02605.
- Haury, L., J. McGowan, and P. Wiebe (1978), *Patterns and Processes in the Time-Space Scales of Plankton Distributions*, Plenum, New York.
- Henson, S., and A. Thomas (2007a), Phytoplankton scales of variability in the California Current System: 2. Latitudinal variability, *J. Geophys. Res.*, **112**, C07018, doi:10.1029/2006JC004040.
- Henson, S., and A. Thomas (2007b), Phytoplankton scales of variability in the California Current System: 1. Interannual and cross-shelf variability, *J. Geophys. Res.*, **112**, C07017, doi:10.1029/2006JC004039.
- Hickey, B. M., and N. S. Banas (2003), Oceanography of the U.S. Pacific northwest coastal ocean and estuaries with application to coastal ecology, *Estuaries Coasts*, **26**(4), 1010–1031, doi:10.1007/BF02803360.
- Hickey, B. M., and N. S. Banas (2008), Why is the northern end of the California Current System so productive?, *Oceanography*, **21**(4), 90–107, doi:10.5670/oceanog.2008.07.
- Hickey, B. M., S. Geier, N. Kachel, and A. MacFadyen (2005), A bi-directional river plume: The Columbia in summer, *Cont. Shelf Res.*, **25**(14), 1631–1656, doi:10.1016/j.csr.2005.04.010.
- Hoge, F. E., C. W. Wright, P. E. Lyon, R. N. Swift, and J. K. Yungel (1999), Satellite retrieval of inherent optical properties by inversion of an oceanic radiance model: A preliminary algorithm, *Appl. Opt.*, **38**(3), 495–504, doi:10.1364/AO.38.000495.
- Hoge, F., P. Lyon, R. Swift, J. Yungel, M. Abbott, R. Letelier, and W. Esaias (2003), Validation of Terra-MODIS phytoplankton chlorophyll fluorescence line height: I. Initial airborne lidar results, *Appl. Opt.*, **42**(14), 2767–2771.
- Hu, C., F. E. Muller-Karger, G. A. Vargo, M. B. Neely, and E. Johns (2004), Linkages between coastal runoff and the Florida Keys ecosystem: A study of a dark plume event, *Geophys. Res. Lett.*, **31**, L15307, doi:10.1029/2004GL020382.
- Hu, C., F. E. Muller-Karger, C. J. Taylor, K. L. Carder, C. Kelble, E. Johns, and C. A. Heil (2005), Red tide detection and tracing using MODIS fluorescence data: A regional example in SW Florida coastal waters, *Remote Sens. Environ.*, **97**(3), 311–321, doi:10.1016/j.rse.2005.05.013.
- Huyer, A. (1983), Coastal upwelling in the California Current system, *Prog. Oceanogr.*, **12**(3), 259–284, doi:10.1016/0079-6611(83)90010-1.
- International Ocean-Colour Coordinating Group (2000), Remote sensing of ocean colour in coastal, and other optically complex, waters, in *Reports of the International Ocean-Colour Coordinating Group, Group, Rep. 3*, edited by S. Sathyendranath, Dartmouth, NS, Canada.
- Kiefer, D. A., and R. A. Reynolds (1992), *Advances in Understanding Phytoplankton Fluorescence and Photosynthesis*, Plenum, New York.
- Large, W., and S. Pond (1981), Open ocean momentum flux measurements in moderate to strong winds, *J. Phys. Oceanogr.*, **11**(3), 324–336, doi:10.1175/1520-0485(1981)011<0324:OOMFMI>2.0.CO;2.
- Letelier, R. M., and M. R. Abbott (1996), An analysis of chlorophyll fluorescence algorithms for the Moderate Resolution Imaging Spectrometer (MODIS), *Remote Sens. Environ.*, **58**(2), 215–223, doi:10.1016/S0034-4257(96)00073-9.
- Maritorena, S., D. A. Siegel, and A. R. Peterson (2002), Optimization of a semianalytical ocean color model for global-scale applications, *Appl. Opt.*, **41**(15), 2705–2714, doi:10.1364/AO.41.002705.
- O'Reilly, J. E., S. Maritorena, B. G. Mitchell, D. A. Siegel, K. L. Carder, S. A. Garver, M. Kahru, and C. McClain (1998), Ocean color chlorophyll algorithms for SeaWiFS, *J. Geophys. Res.*, **103**, 24,937, doi:10.1029/98JC02160.
- Phillips, E. M., J. E. Zamon, H. M. Nevins, C. M. Gobble, R. S. Duerr, and L. H. Kerr (2011), Summary of birds killed by a harmful algal bloom along the south Washington and north Oregon coasts during October 2009, *Northwest. Nat.*, **92**(2), 120–126, doi:10.1898/10-32.1.
- Pierce, S. D., J. A. Barth, R. E. Thomas, and G. W. Fleischer (2006), Anomalous warm July 2005 in the northern California Current: Historical context and the significance of cumulative wind stress, *Geophys. Res. Lett.*, **33**, L22S04, doi:10.1029/2006GL027149.
- Siegel, D., S. Doney, and J. Yoder (2002a), The North Atlantic spring phytoplankton bloom and Sverdrup's critical depth hypothesis, *Science*, **296**(5568), 730–733, doi:10.1126/science.1069174.
- Siegel, D. A., S. Maritorena, N. B. Nelson, D. A. Hansell, and M. Lorenzi-Kayser (2002b), Global distribution and dynamics of colored dissolved and detrital organic materials, *J. Geophys. Res.*, **107**(C12), 3228, doi:10.1029/2001JC000965.
- Siegel, D. A., S. Maritorena, N. B. Nelson, M. J. Behrenfeld, and C. R. McClain (2005), Colored dissolved organic matter and its influence on the satellite-based characterization of the ocean biosphere, *Geophys. Res. Lett.*, **32**, L20605, doi:10.1029/2005GL024310.
- Smayda, T. J. (1997), What is a bloom? A commentary, *Limnol. Oceanogr.*, **42**(5), 1132–1136, doi:10.4319/lo.1997.42.5 part 2.1132.
- Trainer, V. L., G. C. Pitcher, B. Reguera, and T. J. Smayda (2010), The distribution and impacts of harmful algal bloom species in eastern boundary upwelling systems, *Prog. Oceanogr.*, **85**(1–2), 33–52, doi:10.1016/j.pocean.2010.02.003.
- Tweddle, J. F., et al. (2010), Relationships among upwelling, phytoplankton blooms, and phycotoxins in coastal Oregon shellfish, *Mar. Ecol. Prog. Ser.*, **405**, 131–145, doi:10.3354/meps08497.
- Venegas, R., P. Strub, E. Beier, R. Letelier, A. Thomas, T. Cowles, C. James, L. Soto-Mardones, and C. Cabrera (2008), Satellite-derived variability in chlorophyll, wind stress, sea surface height, and temperature in the northern California Current System, *J. Geophys. Res.*, **113**, C03015, doi:10.1029/2007JC004481.
- Ware, D. M., and R. E. Thomson (1991), Link between long-term variability in upwelling and fish production in the northeast Pacific Ocean, *Can. J. Fish. Aquat. Sci.*, **48**(12), 2296–2306, doi:10.1139/f91-270.
- Ware, D. M., and R. E. Thomson (2005), Bottom-up ecosystem trophic dynamics determine fish production in the northeast Pacific, *Science*, **308**(5726), 1280–1284, doi:10.1126/science.1109049.
- Werdell, P., and S. Bailey (2005), An improved in-situ bio-optical data set for ocean color algorithm development and satellite data product validation, *Remote Sens. Environ.*, **98**(1), 122–140, doi:10.1016/j.rse.2005.07.001.
- Werdell, P., B. Franz, S. Bailey, L. Harding, and G. Feldman (2007), Approach for the long-term spatial and temporal evaluation of ocean color satellite data products in a coastal environment, *Proc. SPIE Int. Soc. Opt. Eng.*, **6680**, 1–12.
- Wetz, M., B. Hales, Z. Chase, P. Wheeler, and M. Whitney (2006), Riverine input of macronutrients, iron, and organic matter to the coastal ocean off Oregon, USA, during the winter, *Limnol. Oceanogr.*, **51**(5), 2221–2231, doi:10.4319/lo.2006.51.5.2221.
- Wilson, C. (2003), Late summer chlorophyll blooms in the oligotrophic North Pacific subtropical gyre, *Geophys. Res. Lett.*, **30**(18), 1942, doi:10.1029/2003GL017770.